

Space-Time Phononic Crystals with Anomalous Topological Edge States

Mourad Oudich^{1,2,*}, Yuanchen Deng¹, Molei Tao³, and Yun Jing^{1,*}

¹*Department of Mechanical and Aerospace Engineering, North Carolina State University, Raleigh, North Carolina 27695, USA*

²*Université de Lorraine, CNRS, Institut Jean Lamour, F-54000 Nancy, France*

³*School of Mathematics, Georgia Institute of Technology, Atlanta, Georgia 30332, USA*

* moudich@ncsu.edu , yjing2@ncsu.edu

Abstract

It is well known that an interface created by two topologically distinct structures could potentially host nontrivial edge states that are immune to defects. In this letter, we introduce a one-dimensional space-time phononic crystal and study the associated anomalous topological edge states. The space-coupled time modulation, while preserving the key topological feature of the system, also duplicates the edge state mode across the spectrum, both inside and outside the band gap. It is shown that, in contrast to conventional topological edge states which are excited by frequencies in the Bragg regime, the space-time-modulation-induced frequency conversion can be leveraged to access topological edge states at a deep subwavelength scale where the phononic crystal size is merely 1/55 of the wavelength. This remarkable feature, in conjunction with the non-reciprocity introduced by the time modulation, could open a new route for designing miniature devices that are based on topological physics.

There has been a growing interest in topological phases since the discovery of topological insulators in quantum physics. One of the most intriguing phenomena associated with topological phases is the topological edge state, which is symmetry-protected and is immune to local material imperfections. Topological phases have also recently been identified in classical systems such as in photonics [1-11], acoustics [12-28], and mechanics [29-33]. These topological phases harbor nontrivial wave modes that are stable against local perturbations, offering an ingenious solution for realizing robust, backscattering-immune wave propagation [12-23] as well as energy localization [24-28]. While most recent studies pertaining to topological edge states have focused on two-dimensional (2D) [12-20,27-33] or even three-dimensional (3D) systems [21-23], one-dimensional (1D) systems [24-26] could serve as a simpler yet versatile platform for enhancing our fundamental knowledge on topological physics. For the 1D case, the topological phase (or geometrical phase) of the bulk band is specifically known as the Zak phase [34,35]. Considering a design of periodic structure with a band gap (BG), it is discovered that the continuous deformation of the structure with constant symmetry can produce closing and opening of the BG supported by a topological phase transition. This phase transition can be leveraged to design

topologically protected edge states that reside between the initial structure and a deformed one. Xiao *et. al* [24] demonstrated this mechanism in a 1D acoustic system where a topological edge state was created between two phononic crystals (PC) having topologically distinct BGs. Meanwhile, topological edge states are dictated by the geometrical symmetry of the system and occur at the topological BG where the wavelength is comparable with the structure periodicity [17]. This limits their functionalities to the Bragg scattering regime. One critical consequence, for instance, is that the resulting structure can be very bulky at low frequencies. This letter introduces a new strategy to break down this barrier by imposing both space and time modulation (STM) on the medium properties. The STM could enable the engineering of topological phases in the time domain which provides an extra degree of freedom and therefore richer physics. There are two major findings in this study: (1) the creation of anomalous topological edge states in the bulk band; (2) the possibility to excite the edge state in the Bragg regime using ultralow frequencies whose wavelengths could be orders of magnitude greater than the periodicity of the PC. Furthermore, the proposed approach could have implications for unidirectional sensing as well as filtering, which are enabled by the partnership between the non-reciprocity of the system and anomalous topological edge states. These features could bring about new designs of miniature devices based on topological phases for unconventional wave manipulation, excitation, and detection. Although the current study focuses on 1D acoustic systems, the theory developed here can readily be extended to higher dimensions and other wave-based systems.

STM of the medium properties has been proposed as a robust way to break reciprocity which is an intrinsic property of wave dynamics in conventional systems. Consequently, non-identical wave transmission in opposite directions can be achieved. Space-time (ST) photonic crystals were in fact introduced decades ago [36-38] and the subject on non-reciprocity has recently been reinvigorated in the field of photonics for the control of electromagnetic waves using time-variation of permittivity and/or permeability [39-43]. There has also been numerous works regarding STM in acoustics [44,45] and elastic waves where elastic properties of the medium are ST modulated to achieve nonreciprocal wave propagation [46-48]. Meanwhile, it has been shown that external time-dependent perturbations can be used to achieve topological spectra in initially trivial systems at the equilibrium [6,16,49]. This class of systems is known to be the basis of Floquet topological insulators where time-periodic potential is introduced to a Hermitian system which leads to nontrivial duplicated edge states in the band structure [50-52].

In this work, in contrast to the approach for building Floquet topological insulators, we start from a stationary 1D system possessing nontrivial topological phases as well as topologically protected edge states inside a BG. This initial system is constructed from two PCs exhibiting different Zak phases, i.e., 0 and π . We then introduce a space-coupled time modulation into both PCs in a way that the Zak phase difference between the two PCs remains unchanged throughout the entire duration of time modulation [51]. The resulting PC is referred to as the space-time PC: a “living” PC that evolves in time. As will be

shown below, frequency conversion occurs in the space-time PC, which gives rise to the duplication of edge states across the entire temporal spectrum. This is the underlying physics for the anomalous edge state discovered in this study.

We first consider two PCs having a sinusoidal space modulation of the medium density $\rho(x)$. The governing equations in acoustics in 1D then read [53]:

$$\begin{aligned}\frac{\partial p}{\partial x} &= -\rho(x) \frac{\partial v}{\partial t} \\ \frac{\partial v}{\partial x} &= -K_e \frac{\partial p}{\partial t}\end{aligned}\quad (1)$$

where p , v , ρ and K_e are the pressure, the particle velocity, the density, and the compressibility of the medium. This study assumes K_e to be a constant, i.e., space-and-time independent, though we can conduct a similar study where the density is constant and K_e is space-and-time dependent.

The top left panels of Figs.1(a) and (b) illustrate the unit cell for each PC: one has a modulation in the form of $\rho = \rho_0(1 - \alpha \cos(k_m x))$ and the other is $\rho = \rho_0(1 + \alpha \cos(k_m x))$ in the spatial domain $[0, \lambda_m]$, where $\lambda_m = 2\pi/k_m$ is the space period, ρ_0 is the air density (1.2 kg/m^3), and α is the modulation amplitude (chosen as $\alpha = 0.5$ throughout this study). The two PCs are exactly 180° out of phase in space. Both PCs have the identical band structures (BSs) with a BG around the normalized frequency $\Omega=0.5$ between the first and second bands (bottom left panels of Figs.1 (a) and (b)). For each PC, we plot in the right panels of Figs.1(a) and (b) the acoustic pressure distributions along the unit cell at the edge of the Brillouin zone (BZ) for the first band (point 1), and at both the edge and center of the BZ for the second band (points 2 and 2'). The symmetry of the eigenmode dictates the Zak phase of each band. For instance, for the first PC in Fig.1 (a), points 2 and 2' in the second band have the same symmetry, indicating a zero Zak phase; for the second PC in Fig. 2 (b), however, different symmetries (anti-symmetrical vs. symmetrical) are present, meaning that the Zak phase is π . The Zak phase can be also confirmed by using the following formula [24]:

$$\theta_Z = \int_{-\pi/\lambda_m}^{\pi/\lambda_m} \langle u_k | \partial_k | u_k \rangle dk = \frac{1}{2\rho_0 c_0^2} \int_{-\pi/\lambda_m}^{\pi/\lambda_m} \left(i \int_0^{\lambda_m} u_k^*(x) \partial_k u_k(x) dx \right) dk, \quad (2)$$

where k is the wave number and $u_k = e^{-ikx} p$.

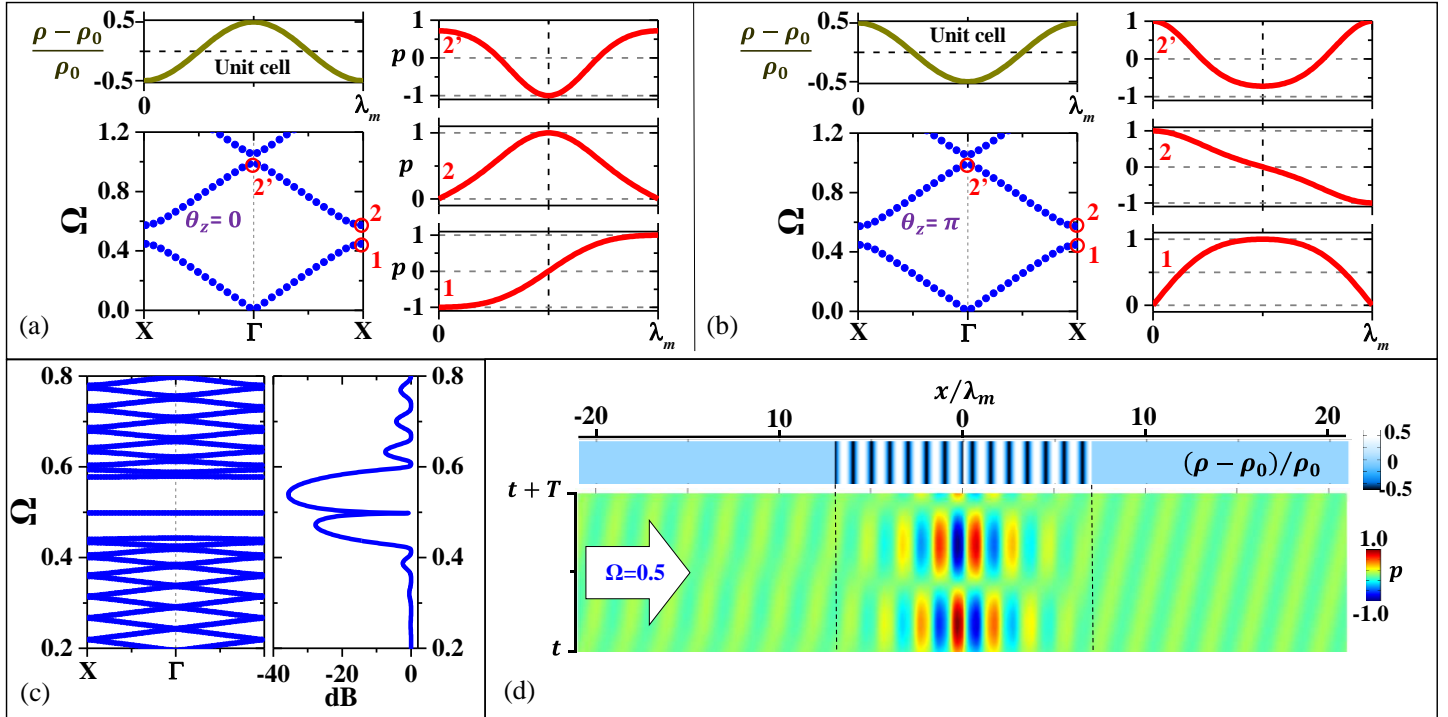


Fig1. (a) A stationary PC with density modulation of $\rho = \rho_0(1 - \alpha \cdot \cos(k_m x))$ along the unit cell $[0, \lambda_m]$ and its band structure (bottom left panel). Pressure fields are also plotted for the eigenmodes indicated by 1, 2 and 2' in the band structure (right panels). (b) Same as (a) but for the second stationary PC with density modulation of $\rho = \rho_0(1 + \alpha \cdot \cos(k_m x))$. (c) Band structure for the system constructed by the two PCs where each PC is made of 7 unit cells: $\rho = \rho_0(1 - \alpha \cdot \cos(k_m x))$ for $x < 0$ and $\rho = \rho_0(1 + \alpha \cdot \cos(k_m x))$ for $x > 0$. The corresponding transmission spectrum is shown on the right, where an edge state with a high transmission can be observed at $\Omega=0.5$. (d) (Top panel) Transmission configuration along the system and (bottom panel) the edge state pressure field for a single frequency excitation plotted against the time. In both panels, the vertical axis is the time and the horizontal axis is the space.

Taking advantage of the Zak phase change in the second band, a topological edge state located at $x = 0$ using both PCs is constructed. The resulting system has a space modulation of $\rho = \rho_0(1 - \alpha \cdot \cos(k_m x))$ for $x < 0$ and $\rho = \rho_0(1 + \alpha \cdot \cos(k_m x))$ for $x > 0$. The BS and the transmission spectrum of this system are plotted in Fig.1(c) which both show the existence of an edge state. The calculations are performed in the frequency domain using the commercial software Comsol Multiphysics® v5.3a. This edge state is located at the middle of the Bragg BG, i.e., $\Omega = \omega/k_m c_0 = 0.5$, at which the structure periodicity corresponds to half of the wavelength. We plot in the top panel of Fig.1 (d) the density distribution of the system in a transmission configuration where each PC consists of 7 unit cells (14 in total). For a monochromatic wave excitation at the edge state frequency $\Omega = 0.5$, the pressure field distribution (real part of the complex pressure) is plotted in Fig.1 (d) during one time period $T = 2\pi/\omega$. The acoustic energy is clearly confined in the vicinity of the interface between the two PCs ($x=0$). It is noted that although sinusoidal modulation is chosen in this study, the theory

developed here can be generalized to other types of modulation (e.g., square modulation) and the main physical observation is expected to be the same.

Time modulation is subsequently introduced to both PCs following $\rho = \rho_0(1 - \alpha \cos(\omega_m t - k_m x))$ for $x < 0$ and $\rho = \rho_0(1 + \alpha \cos(\omega_m t - k_m x))$ for $x > 0$. A modulation frequency of $\Omega_m = \omega_m/k_m c_0 = 0.2$ is chosen. Please note that the density is not assumed to be weakly modulated as was done in [45]. This time modulation is space-coupled in the sense that both ST modulations appear in the cosine function. Discussions regarding space-decoupled time modulation, which is largely unexplored, can be found in the supplementary material where the fundamental differences between the two modulation modalities are delineated [54]. One major difference is that only the space-coupled modulation breaks the reciprocity. This is because under such a modulation, the density variation can be manifested as a wave propagating in either positive or negative x -direction, and this synthetic external field is the foundation of the mechanism that breaks the symmetry of the system. With the space-coupled time modulation, each PC has its Zak phase changing with time in a way that the Zak phase difference remains constant between the two PCs. Figure 2 displays the Zak phase variation against time for each PC during one modulation period $T_m = 2\pi/\omega_m$, where we can clearly see that the Zak phase difference between the two PCs remains constant at π , indicating the existence of edge states at each time instant.

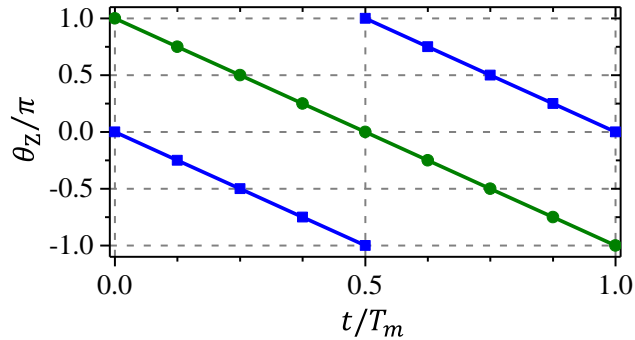


Fig.2. Zak phase θ_z as a function of time for both PCs during one modulation period. The blue line is for the first PC with the modulation of $\rho = \rho_0(1 - \alpha \cos(\omega_m t - k_m x))$ while the green line is for the second PC with the modulation of $\rho = \rho_0(1 - \alpha \cos(\omega_m t - k_m x))$. The difference between the two Zak phases remains unchanged and equals to π .

The top panel of Fig. 3 (b) shows the density variation during one modulation period $T_m = 2\pi/\omega_m$ where the topological system is made of 14 unit cells, same as in the stationary case. Indeed, the density variation can be seen as a wave traveling in the $+x$ direction as time progresses. Figure 3(a) illustrates the calculated transmission spectrum for forward wave propagation (from left to right). The calculation is performed by COMSOL in the time domain where we analyze the Fourier spectrum of the transmitted wave through the structure for a wideband incident pulse. Compared to the stationary case, the BG under STM is shifted to higher frequencies by $\Omega_m/2 = 0.1$. It was previously shown that this type of time modulation could introduce asymmetrical BG shift for opposite propagation directions which can be

used to achieve one way propagation [46]. In Fig. 3 (a), a transmission peak is observed inside this BG at the normalized frequency $\Omega=0.6013$, corresponding to the excitation of the edge state which is also shifted from its initial frequency in the case of the stationary system ($\Omega=0.5$). We also note two transmission dips at $\Omega=0.2013$ and 0.4013 as well as a peak at 0.8013 and all of them are outside the BG. These are in fact edge state modes, and their emergence in the bulk band can be attributed to the STM-induced frequency conversion, which changes the topological feature of the structure leading to duplicated edge states at frequencies $\Omega_0 \pm n\Omega_m$ [50-52]. Interestingly, the transmission characteristic of the system for backward wave propagation is dramatically different due to the non-reciprocity of the system. For example, the edge state (transmission peak) at $\Omega=0.6013$ vanishes. As shown in the supplementary material, this highly asymmetrical behavior can be utilized for applications such as unidirectional sensing or filtering.

To gain a better insight on these modes, the bottom panels of Fig. 3(b) show the wave pressure fields for monochromatic excitations at frequencies $\Omega_0 = 0.6013$ and $\Omega_0 - \Omega_m = 0.4013$, where one can observe localized modes at the interface. These modes, however, are not pure in Fourier components, although the excitation is strictly monochromatic. To this end, we apply temporal Fourier transform to the wave field shown in Fig. 3(b) and the results (referred to as the spatial-frequency spectrum of the wave field) are presented in Fig. 3(c) for the case of $\Omega_0 = 0.6013$ and $\Omega_0 - \Omega_m = 0.4013$, respectively plotted in the left and right panels. In other words, these are the pressure fields along the PC at different frequencies. The spatial domain has a range of $-20 < x/\lambda_m < 20$. In the case of an incident wave at $\Omega_0 = 0.6013$ (left panel of Fig. 3(c)), an edge state mode confined at the center of the system (in the vicinity of $x=0$) is excited at $\Omega_0 = 0.6013$ but also at $\Omega_0 - \Omega_m = 0.4013$ which is outside the BG. A second order edge state is also excited at $\Omega_0 - 2\Omega_m = 0.2013$ but is less visible since the energy allocated at higher order edge states is weaker. These edge states at $\Omega_0 - n\Omega_m$ are considered anomalous edge states since for stationary PCs, the edge state only appears in the BG. Meanwhile, if we choose a monochromatic excitation exactly at $\Omega_0 - \Omega_m = 0.4013$, the wave fields plotted in the right panel of Fig. 3(c) suggest that, not only the excitation of an edge state at this frequency ($\Omega=0.4013$) is possible, but also an edge state at $\Omega_0 = 0.6013$ inside the BG can be excited.

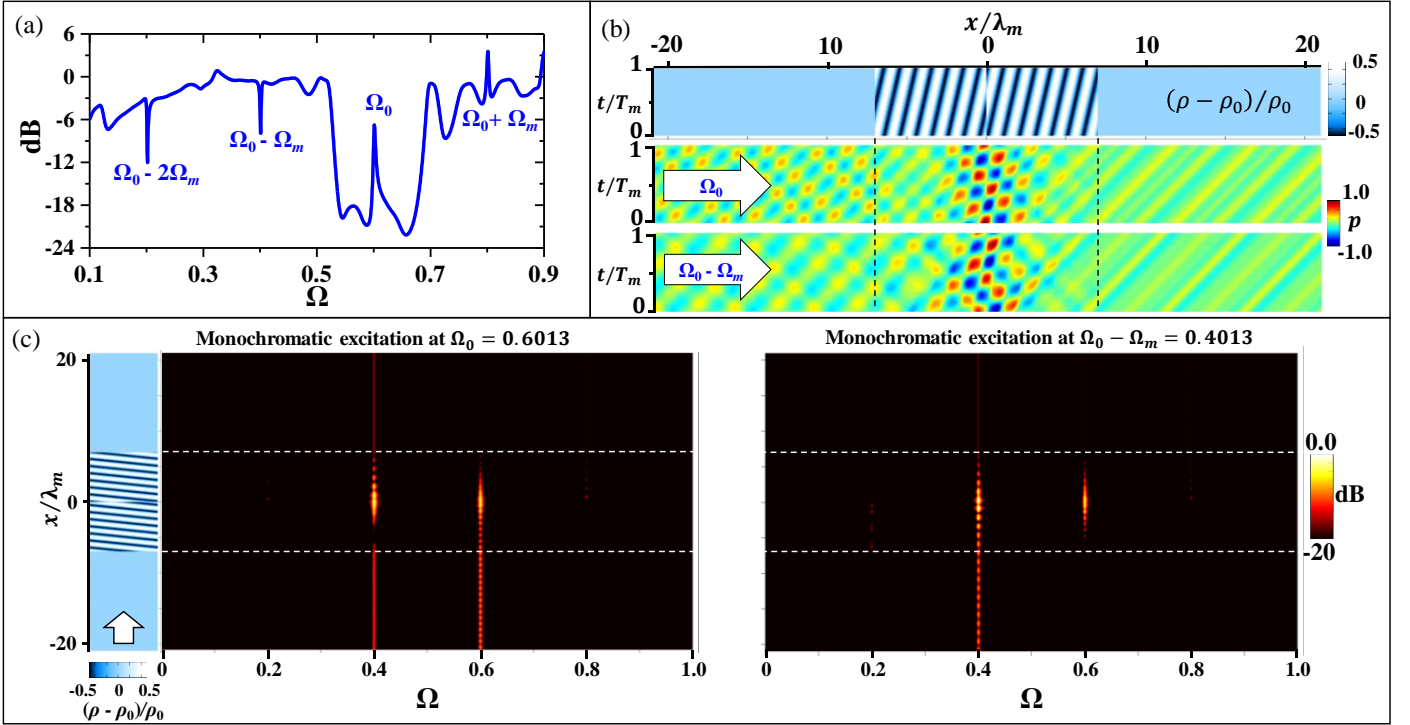


Fig.3. (a) Transmission spectrum through the ST modulated system composed of two PCs with a constant Zak phase shift. (b) (Top panel) Transmission configuration of the structure with density modulation of $\rho = \rho_0(1 - \alpha \cdot \cos(\omega_m t - k_m x))$ for $x < 0$ and $\rho = \rho_0(1 + \alpha \cdot \cos(\omega_m t - k_m x))$ for $x > 0$ presented within one modulation period T_m . (Bottom panels) Pressure fields for incident wave at $\Omega_0 = 0.6013$ and $\Omega_0 - \Omega_m = 0.4013$, respectively. (c) Spatial-frequency spectra of the wave field for incident wave excitations at $\Omega_0 = 0.6013$ (left panel) and $\Omega_0 - \Omega_m = 0.4013$ (right panel).

To further generalize this observation, we explore the possibility to excite the edge state located at Ω_0 by excitation frequencies of $\Omega_0 - n\Omega_m$. Indeed, with the monochromatic excitation at $\Omega_0 - \Omega_m$, we can excite the edge state at Ω_0 , as shown in Fig. 3. In this case, the acoustic wavelength is comparable with the structure periodicity, i.e., $\lambda = 2.49\lambda_m$. Figure 4 (a) shows the spatial-frequency spectrum of the wave field when the monochromatic excitation is at $\Omega_0 - 2\Omega_m = 0.2013$, where the excitation of the first and 2nd order edge states at $\Omega_0 - \Omega_m$ and Ω_0 can be clearly observed, respectively. In this case, the incident wavelength is $\lambda = 4.97\lambda_m$, which can be compared with the stationary PC where the edge state is excited by a wavelength $\lambda = 2\lambda_m$. Remarkably, we can also excite multiple edge states by pumping acoustic energy at an ultra-low frequency, i.e., $\Omega_0 - 3\Omega_m = 0.0013$. Figure 4(b) shows the spatial-frequency spectrum of the wave field for this excitation where the incident wavelength is $\lambda = 769\lambda_m$. The excitation of the edge state at $\Omega_0 = 0.6013$ located in the Bragg regime is evident, although the color bar was redrawn in order to more clearly illustrate this third order edge state. As the entire modulated system has a length of $L_s = 14\lambda_m$, the system is functional even though its size is merely 1/55 of the wavelength λ . While time modulation has the potential to enable deep subwavelength excitations of Bragg-associated functionalities, it must be pointed out that high order edge states (e.g., the one at $\Omega_0 = 0.6013$) intrinsically suffer from poor efficiency. In the last example, the peak pressure in the third order edge state is about 69 dB lower than that of the zeroth order edge state. In practice, this signal could be buried in noise. To overcome this limitation without changing the deep subwavelength footprint, one would need to push the first order edge state which has higher efficiency

into very low frequency range. This can be done by increasing the modulation frequency Ω_m . However, the BG closes for very high Ω_m in the case of space-coupled time modulation. The solution is to use space-decoupled time modulation, where the topological BG is not affected by increasing Ω_m . A design based on this strategy is provided in the supplementary material [54] where the 1st order edge state is excited and the PC periodicity λ_m is $\lambda/71$. More importantly, the peak pressure in the first order edge state is only about 26 dB lower than that of the zeroth order edge state. One pitfall of this design, though, is that the non-reciprocity feature is lost.

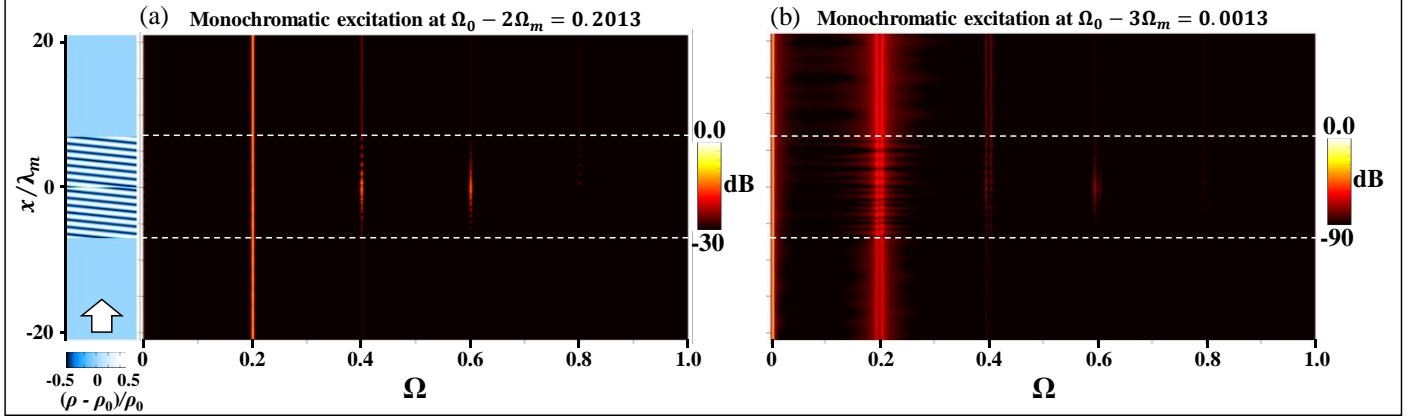


Fig.4. Spatial-frequency spectra of the wave fields for incident wave excitations at (a) $\Omega_0 - 2\Omega_m = 0.2013$ and (b) $\Omega_0 - 3\Omega_m = 0.0013$. In both cases, topological edge states are higher frequencies can be excited.

In conclusion, we propose to enrich the functionalities of topological devices via time modulation, which gives rise to the duplication of topological edge states across the entire spectrum. This feature can be used to achieve deep subwavelength manipulation of the edge state in the Bragg regime, which could be proven useful for designing miniature topological devices for wave guiding, sensing, and excitation, among other intriguing functionalities. Furthermore, the STM studied in this work introduces non-reciprocity to the system which could engender exotic unidirectional wave behaviors. Future work will expand the model to higher dimensions where even richer physics can be foreseen. It would be also interesting to construct a real physical model to experimentally validate the theory. Active acoustic metamaterials [45] and piezoelectric materials [48] could be viable options in this regard.

References

- [1] F. D. M. Haldane, and S. Raghu. Possible realization of directional optical waveguides in photonic crystals with broken time-reversal symmetry. *Phys. Rev. Lett.* **100**, 013904 (2008)
- [2] M. Hafezi, E. A. Demler, M. D. Lukin, J. M. Taylor. Robust optical delay lines with topological protection. *Nat. Phys.* **7**, 907 (2011)
- [3] K. Fang, Z. Yu, and S. Fan. Realizing effective magnetic field for photons by controlling the phase of dynamic modulation. *Nat. Photonics*, **6**, 782 (2012)

- [4] L.-H. Wu, and X. Hu, Scheme for Achieving a Topological Photonic Crystal by Using Dielectric Material. *Phys. Rev. Lett.* **114**, 223901 (2015)
- [5] A. B. Khanikaev, S. H. Mousavi, W.-K. Tse, M. Kargarian, A. H. MacDonald, G. Shvets. Photonic topological insulators. *Nat. Materials* **12**, 233 (2013)
- [6] M. C. Rechtsman, J. M. Zeuner, Y. Plotnik, Y. Lumer, D. Podolsky, F. Dreisow, S. Nolte, M. Segev, and A. Szameit. Photonic Floquet topological insulators. *Nature*, **496**, 196 (2013)
- [7] L. Lu, J. D. Joannopoulos, M. Soljačić. Topological photonics. *Nat. Photonics* **8**, 821 (2014)
- [8] Y. Plotnik, M. C. Rechtsman, D. H. Song, M. Heinrich, J. M. Zeuner, S. Nolte, Y. Lumer, N. Malkova, J. Xu, A. Szameit, Z. Chen, and M. Segev. Observation of unconventional edge states in 'photonic graphene'. *Nat. Materials*. **13**, 57 (2014)
- [9] S. A. Skirlo, L. Lu, M. Soljačić. Multimode One-Way Waveguides Of Large Chern Numbers. *Phys. Rev. Lett.* **113**, 113904 (2014)
- [10] S. A. Skirlo, L. Lu, Y. C. Igarashi, Q. H. Yan, J. Joannopoulos, M. Soljačić. Experimental Observation of Large Chern Numbers in Photonic Crystals. *Phys. Rev. Lett.* **115**, 253901 (2015)
- [11] T. Ozawa, H. M. Price, A. Amo, N. Goldman, M. Hafezi, L. Lu, M. C. Rechtsman, D. Schuster, J. Simon, O. Zilberberg, and I. Carusotto. Topological photonics. *Rev. Mod. Phys.* **91**, 015006 (2019)
- [12] Z. Yang, F. Gao, X. Shi, X. Lin, Z. Gao, Y. Chong, and B. Zhang. Topological Acoustics. *Phys. Rev. Lett.* **114**, 114301 (2015)
- [13] X. Ni, C. He, X.-C. Sun, X.-P. Liu, M.-H. Lu, L. Feng, and Y.-F. Chen. Topologically protected one-way edge mode in networks of acoustic resonators with circulating air flow. *New J. Phys.* **17**, 053016 (2015)
- [14] A. B. Khanikaev, R. Fleury, S. H. Mousavi, and A. Alù. Topologically robust sound propagation in an angular-momentum-biased graphene-like resonator lattice. *Nat. Comm.* **6**, 8260 (2015)
- [15] C. He, X. Ni, H. Ge, X.-C. Sun, Y.-B. Chen, M.-H. Lu, X.-P. Liu and Y.-F. Chen. Acoustic topological insulator and robust one-way sound transport. *Nat. Phys.* **12**, 1124 (2016)
- [16] R. Fleury, A. B. Khanikaev, and A. Alù. Floquet topological insulators for sound. *Nat. Comm.* **7**, 11744 (2016)
- [17] Z.-G. Chen, and Y. Wu, Tunable topological phononic crystals. *Phys. Rev. Appl.* **5**, 054021 (2016).
- [18] Y. Deng, H. Ge, Y. Tian, M. Lu, and Y. Jing. Observation of zone folding induced acoustic topological insulators and the role of spin-mixing defects. *Phys. Rev. B* **96**, 184305 (2017)
- [19] X. Zhang, M. Xiao, Y. Cheng, M.-H. Lu, and J. Christensen, Topological sound. *Communications Physics*, **1**, 97 (2018)
- [20] G. Ma, M. Xiao, and C. T. Chan. Topological phases in acoustic and mechanical systems. *Nat. Rev. Phys.* **1**, pages281–294 (2019)
- [21] H. Ge, X. Ni, Y. Tian, S. K. Gupta, M.-H. Lu, X. Lin, W.-D. Huang, C. T. Chan, and Y.-Fe. Chen. Experimental Observation of Acoustic Weyl Points and Topological Surface States. *Phys. Rev. Appl.* **10**, 014017 (2018)

- [22] C. He, S.-Y. Yu, H. Ge, H. Wang, Y. Tian, H. Zhang, X.-C. Sun, Y. B. Chen, J. Zhou, M.-H. Lu, and Y.-F. Chen. Three-dimensional topological acoustic crystals with pseudospin-valley coupled saddle surface states. *Nat. Comm.* **9**, 4555 (2018)
- [23] F. Li, X. Huang, J. Lu, J. Ma, and Z. Liu. Weyl points and Fermi arcs in a chiral phononic crystal. *Nat. Phys.* **14**, 30 (2018)
- [24] M. Xiao, G. Ma, Z. Yang, Ping Sheng, Z. Q. Zhang & C. T. Chan, Geometric phase and band inversion in periodic acoustic systems. *Nat. Phys.* **11**, 240 (2015)
- [25] X. Li Yan Meng, X. Wu, S. Yan, Y. Huang, S. Wang, and W. Wen, Su-Schrieffer-Heeger model inspired acoustic interface states and edge states. *Appl. Phys. Lett.* **113**, 203501 (2018)
- [26] W. Zhu, X. Fang, D. Li, Y. Sun, Y. Li, Y. Jing, and H. Chen. Simultaneous Observation of a Topological Edge State and Exceptional Point in an Open and Non-Hermitian Acoustic System. *Phys. Rev. Lett.* **121**, 124501 (2018)
- [27] X. Ni, M. Weiner, A. Alù, and A. B. Khanikaev. Observation of higher-order topological acoustic states protected by generalized chiral symmetry. *Nat. Mat.* **18**, 113 (2019)
- [28] H. Xue, Y. Yang, F. Gao, Y. Chong, and B. Zhang. Acoustic higher-order topological insulator on a kagome lattice *Nat. Mat.* **18**, 108 (2019)
- [29] S. H. Mousavi, A. B. Khanikaev, and Z. Wang. Topologically protected elastic waves in phononic metamaterials. *Nat. Commun.* **6**, 8682 (2015)
- [30] S.-Y. Yu, C. He, Z. Wang, F.-K. Liu, X.-C. Sun, Z. Li, H.-Z. Lu, M.-H. Lu, X.-P. Liu, and Y.-F. Chen, Elastic pseudospin transport for integratable topological phononic circuits. *Nat. Comm.* **9**, 3072 (2018)
- [31] M. Miniaci, R. K. Pal, B. Morvan, and M. Ruzzene, Experimental observation of topologically protected helical edge modes in patterned elastic plates. *Phys. Rev. X* **8**, 031074 (2018)
- [32] M. Yan, J. Lu, F. Li, W. Deng, X. Huang, J. Ma, and Z. Liu, On-chip valley topological materials for elastic wave manipulation, *Nat. Materials* **17**, 993 (2018)
- [33] Z. Wang, F.-K. Liu, S.-Y. Yu, S.-L. Yan, M.-H. Lu, Y. Jing, and Y.-F. Chen. Guiding robust valley-dependent edge states by surface acoustic waves. *J. Appl. Phys.* **125**, 044502 (2019)
- [34] J. Zak. Berry's phase for energy bands in solids. *Phys. Rev. Lett.* **62**, 2747 (1989)
- [35] M. Atala, M. Aidelsburger, J. T. Barreiro, D. Abanin, T. Kitagawa, E. Demler, and I. Bloch. Direct measurement of the Zak phase in topological Bloch bands. *Nat. Phys.* **9**, 795 (2013)
- [36] A. Oliner and A. Hessel, Guided waves on sinusoidally modulated reactance surfaces, *IEEE Trans. Antennas Propag.* **7**, 201 (1959)
- [37] E. S. Casedy and A. A. Oliner, Dispersion relations in time-space periodic media: Part I—Stable interactions, *Proc. IEEE* **51**, 1342 (1963)
- [38] E. S. Casedy, Waves guided by a boundary with time-space periodic modulation, *Proc. IEEE* **112**, 269 (1965)

- [39] Y. Hadad, D. L. Sounas, and A. Alù, Space-time gradient metasurfaces, *Phys. Rev. B* **92**, 100304 (2015).
- [40] Sajjad Taravati, Self-biased broadband magnet-free linear isolator based on one-way space-time coherency, *Phys. Rev. B* **96**, 235150 (2017).
- [41] S. Taravati, N. Chamanara, and C. Caloz, Nonreciprocal electromagnetic scattering from a periodically space-time modulated slab and application to a quasisonic isolator, *Phys. Rev. B* **96**, 165144 (2017)
- [42] S. Taravati, Aperiodic space-time modulation for pure frequency mixing, *Phys. Rev. B* **97**, 115131 (2018)
- [43] S. Taravati, Giant Linear Nonreciprocity, Zero Reflection, and Zero Band Gap in Equilibrated Space-Time-Varying Media. *Phys. Rev. Appl.* **9**, 064012 (2018)
- [44] R. Fleury, D. L. Sounas, and A. Alù, Subwavelength ultrasonic circulator based on spatiotemporal modulation. *Phys. Rev. B* **91**, 174306 (2015)
- [45] J. Li, C. Shen, Y. Xie, S. A. Cummer. Non-reciprocal sound propagation in space-time modulated media. arXiv:1811.04130 (2018)
- [46] G. Trainiti and M. Ruzzene, Non-reciprocal elastic wave propagation in spatiotemporal periodic structures, *New. J. Phys.* **18**, 083047 (2016)
- [47] Y. Wang, B. Yousefzadeh, H. Chen, H. Nassar, G. Huang, and C. Daraio. Observation of Nonreciprocal Wave Propagation in a Dynamic Phononic Lattice. *Phys. Rev. Lett.* **121**, 194301 (2018)
- [48] G. Trainiti, Y. Xia, J. Marconi, G. Cazzulani, A. Erturk, and M. Ruzzene. Time-Periodic Stiffness Modulation in Elastic Metamaterials for Selective Wave Filtering: Theory and Experiment. *Phys. Rev. Lett.* **122**, 124301 (2019)
- [49] N. H. Lindner, G. Refael, and V. Galitski, Floquet topological insulator in semiconductor quantum wells. *Nat. Phys.* **7**, 490 (2011)
- [50] T. Kitagawa, E. Berg, M. Rudner, and E. Demler. Topological characterization of periodically driven quantum systems. *Phys. Rev. B* **82**, 235114 (2010)
- [51] M. S. Rudner, N. H. Lindner, E. Berg, and M. Levin. Anomalous Edge States and the Bulk-Edge Correspondence for Periodically Driven Two-Dimensional Systems. *Phys. Rev. X* **3**, 031005 (2013)
- [52] Z. Cherpakova, C. Jörg, C. Dauer, F. Letscher, M. Fleischhauer, S. Eggert, S. Linden, and G. von Freymann. Depopulation of edge states under local periodic driving despite topological protection. arXiv:1807.02321 (2018)
- [53] P. M. Morse, and K. U. Ingard. *Theoretical acoustics*, McGraw-Hill Book Co., New York (1968)
- [54] See Supplemental Material at (Link) for results regarding backward wave propagation and discussions on space-decoupled time modulation.